Rare Gas Effects on Hyperfine Coupling Constants of BO, AlO, and GaO

Friedrich Grein*

Department of Chemistry, University of New Brunswick, Fredericton, NB E3B6E2, Canada

Received: June 1, 2005; In Final Form: July 19, 2005

Using density functional theory methods and large basis sets, we calculated hyperfine coupling constants (HFCCs) for the ^{11}B, ^{17}O, ^{27}Al, and ^{69}Ga nuclei of the radicals BO, AlO, and GaO (XO), embedded in 2−14 rare gas (Rg) Ne and Ar atoms. Kr atoms were included for AlO. The distance of the Rg atoms from XO was varied from 4 to 12 bohr. Matrix effects cause A_{iso}(X) to increase, accompanied by decreases in A_{dip}(X) and A_{dip}(O), while A_{iso}(O) remains close to zero. Changes are largest for AlO, slightly smaller for GaO, and very small for BO, in line with the molecular polarizabilities. Observed changes of A_{iso}(X) and A_{dip}(X) for BO in Ne matrixes and for AlO in Ne, Ar, and Kr matrixes are reproduced in complexes with 12 Rg atoms at distances of 5−6 bohr or 14 Rg atoms at distances of 6−7 bohr. For GaO, experimental data are available only in Ne matrixes. Theoretical results obtained for HFCCs of ^{17}O could not be verified due to insufficient experimental information. Estimates of HFCCs in matrixes not yet experimentally studied and for GaO in the gas phase have been made. Due to the interaction with rare gas atoms, p-spin density on the X and O atoms of XO is converted into s-spin density on X, thereby causing an increase (in magnitude) of A_{iso}(X), accompanied by decreases in A_{dip} of X and O. The higher polarizability of XO along the bond axis is reflected in complexes that have axial Rg atoms showing larger changes in HFCCs than comparable complexes without axial Rg atoms.

Introduction

In a previous paper[1] (paper I), complexes of the rare gases (Rg) Ne and Ar with the radical AlO were investigated by theoretical methods to study changes in the electronic **g**-tensor of AlO due to surrounding rare gas atoms. Matrix effects on properties of atoms and molecules are well-known and are documented in many studies. They have been especially well established in the electron spin resonance spectra of AlO. Knight and Weltner[2] found that $\Delta\mathbf{g}_\perp$ ($\Delta\mathbf{g} = \mathbf{g} - \mathbf{g}_e$) changes from an estimated −1450 ppm in the gas phase[3] to −1900 ppm in Ne, −2600 ppm in Ar, and −5000 ppm in Kr matrixes.

In paper I, the **g**-tensor was calculated for various Rg$_n$−AlO complexes, ranging from 2 to 10 Rg atoms, using perturbation methods based on multireference configuration interaction (MRCI) wave functions, as developed and tested by this group.[4−6] In the Rg−AlO models, various combinations of axially and off-axially placed Rg atoms were used. Axial Rg atoms were placed on the AlO axis, and off-axial ones in one or two rings of four each surrounding the AlO axis. The distance of the Rg atoms from the Al and O atoms (to be detailed later) was varied from 4 to 12 bohr.

It was found that two axial Rg atoms (without additional off-axial ones) generally raise $\Delta\mathbf{g}_\perp$ above the value for free AlO (to less negative values), while rings of Rg atoms lower $\Delta\mathbf{g}_\perp$ below it (to more negative values). For the largest systems studied, having 10 Rg atoms, the biggest changes occur at distances of 5−6 bohr, with $\Delta\mathbf{g}_\perp$'s of −2930 ppm at 5 bohr for Ne and −3530 ppm at 6 bohr for Ar. It was noted that the addition of axial Rg atoms to rings of off-axial ones had a diminishing effect on $|\Delta\mathbf{g}_\perp|$. For example, in the Ne$_8$ series, with two rings of four Ne atoms each, $\Delta\mathbf{g}_\perp$ at 5 bohr is −3230 ppm. When two axial atoms are added, $\Delta\mathbf{g}_\perp$ changes to −2930 ppm (as quoted above), closer to the value of free AlO.

* E-mail: fritz@unb.ca.

In the present work, the effect of rare gas atoms on hyperfine coupling constants (HFCCs) will be investigated. An extension will be made by subjecting not only AlO but also the isovalent molecules BO and GaO to Ne and Ar rare gas environments. Krypton−AlO complexes, for which experimental numbers are available, will be included.

Density functional methods are to be employed for the calculations of HFCCs. Thanks to the shorter computer times required for DFT calculations, compared with those needed for the MRCI methods used in **g**-tensor calculations, the size of the models was increased from 10 to 12 and 14 Rg atoms, the 14-Rg complex having two axial Rg atoms and three rings of four each off-axial ones. They surround the XO (X = B, Al, Ga) radical like a cylinder that is closed if axial atoms are present or open in the absence of the two axial Rg atoms.

Experimental HFCC values for AlO, BO, and GaO[2,7−13] are given in Table 1. A well-pronounced matrix effect is seen for A_{iso}(^{27}Al), which moves from 738 MHz in the gas phase to 766 MHz in a Ne matrix and to 899 MHz in Ar and 920 MHz in Kr. For A_{dip}(^{27}Al), no clear trend can be seen. If anything, there is a small decrease as one goes from the gas phase to the Kr matrix. For BO, the observed change from the gas phase to the Ne matrix value is very small. For GaO, experimental HFCC values could only be found for the Ne matrix, so a matrix effect could not be established from the given experimental number.

Theoretical HFCC values for AlO and GaO have been reported by Knight et al.[8] and by Davidson[14] using unrestricted Hartree−Fock (UHF), restricted open-shell Hartree−Fock (ROHF), and unrestricted Becke three-parameter−Lee, Yang, Parr (UB3LYP) methods; for BO and AlO by Knight et al.[11] using self-consistent field (SCF) and configuration interaction (CI) methods; for BO, AlO, and GaO by Belanzoni et al.[15] using various forms of the zeroth-order regular approximation (ZORA)

10.1021/jp052908n CCC: $30.25
Published on Web 09/21/2005

TABLE 1: Experimental Values for Hyperfine Coupling Constants (MHz) of ^{27}Al, ^{11}B, ^{69}Ga, and ^{17}O Nuclei in AlO, BO, and GaO (XO)

	ref	A_{iso}(X)	A_{dip}(X)	A_{iso}(O)	A_{dip}(O)
BO, gas phase	9	1027.4	27.1		
BO, Ne matrix	10−13	1033(1)	25(1)	−19(3)	−12(3)
AlO, gas phase	7	738.0	56.4		
AlO, Ne matrix	2,8	766(2)	53.0(7)	2	−50
AlO, Ar matrix	2	899(3)	54(1)		
AlO, Kr matrix	2	920(3)	51(1)		
GaO, Ne matrix	8	1483	127	8	−77

method; and for BO and AlO by Engels et al.[16] using the Perdew−Wang exchange functional with the Perdew 1986 correlation functional (PWP86)/individual gauge for localized orbital (IGLO)-III method.

The AlO radical has received much attention in the literature. Yoshimine et al.[17] in 1973 pointed out that the ground state cannot be adequately described by a single-configuration SCF wave function due to a mixture of $Al^{2+}O^{2-}$ and $Al^{+}O^{-}$ contributions, where the unpaired electron resides on Al in the first case and on O in the second. Further discussions are found in Knight et al.,[8] Davidson,[14] and Bruna and Grein.[3] Similar problems have been encountered for the isoelectronic SiO^{+} and GaO.[18]

Several trapping sites could be distinguished for BO in Ne matrixes with motional averaging occurring in the ISO (isotropic) site and strong orientation in the OR (oriented) site.[10−13] However, in Ar matrixes only random orientation is observed.

The effect of Ar, Kr, and Xe matrixes on hyperfine coupling constants and **g**-tensors of atomic boron has been investigated by Kiljunen et al.[19] Eriksson[20] calculated changes to the HFCCs of Mg^{+} and Mg_2^{+} due to surrounding Ne and Ar atoms. The interaction of one Li, Na, or K atom with acetylene and changes to the atomic hyperfine structure were investigated by Eriksson et al.[21]

According to Weltner,[13] in matrixes Δ**g**'s usually become more negative, but hyperfine coupling constants may increase or decrease.

Methods

Hyperfine coupling constants will be given for the ^{11}B, ^{17}O, ^{27}Al, and ^{69}Ga nuclei of BO, AlO, GaO, and their Rg complexes. All three radicals have $^2\Sigma^+$ ground states. The complexes with axial-only Rg atoms have $C_{\infty v}$ symmetry with $^2\Sigma^+$ ground states, while complexes with off-axial rings of Rg atoms have C_{4v} symmetry with $^2A_1$ ground states. HFCCs were calculated using density functional theory methods, which have been shown to give, in general, reliable results. All calculations were performed with the Gaussian03 programs.[22] The basis set was always kept as 6-311+G(3d,f). Bond distances were fixed at the experimental values with 1.6179 Å or 3.057 bohr for AlO, 1.2045 Å or 2.2762 bohr for BO, and 1.7436 Å or 3.2949 bohr for GaO.[23,24] Initially, the B3LYP method was used for both AlO and BO systems. However, A_{iso}(Al) for the AlO molecule calculated with B3LYP is too low, 498.6 MHz, compared with the experimental gas-phase value of 738.0 MHz. Several other methods were tested, including ab initio methods. The results for A_{iso}(Al,O) and A_{dip}(Al,O) of AlO are displayed in Table 2. It is seen that the Møller−Plesset second-order perturbation theory (MP2) and configuration interaction with single and double excitation (CISD) methods lead to poor results. Amazingly, the best fit is obtained with SVWN, one of the earliest density functionals, which combines Slater's local spin density exchange[25] with Vosko, Wilk, and Nusair's local spin density correlation functional.[26] The SVWN result for A_{iso}(Al) of AlO is 742.4 MHz, very close to the experimental gas-phase value. Using

TABLE 2: Hyperfine Coupling Constants (MHz) for AlO Calculated by Various ab Initio and Density Functional Methods[a]

	^{27}Al		^{17}O	
	A_{iso}	A_{dip}	A_{iso}	A_{dip}
UHF	571.1	56.2	16.5	−54.4
UMP2	10.4	74.3	135.5	−52.6
UCISD	−50.0	66.7	63.6	−69.6
USVWN	742.4	57.7	19.2	−54.4
USVWN5	730.0	57.5	19.4	−54.6
UB3LYP	498.2	60.3	13.5	−64.5
UB3PW91	529.1	58.4	26.0	−60.7
UMPW1PW91	492.2	58.6	27.1	−61.5
UPW91PW91	625.8	57.0	20.8	−58.2
expt	738.0[b]	56.4[b]	2[c]	−50[c]

[a] The basis set is always 6-311+G(3d,f). UHF = unrestricted Hartree−Fock; UMP2 = unrestricted Møller−Plesset second-order perturbation theory; UCISD = unrestricted configuration interaction with single and double excitation; USVWN = unrestricted Slater's local spin density exchange with Vosko, Wilk, and Nusair's local spin density correlation functional; UB3LYP = unrestricted Becke three-parameter with Lee, Yang, Parr method; UB3PW91 = unrestricted Becke three-parameter with Perdew−Wang 1991 method; UMPW1PW91 = unrestricted modified Perdew−Wang exchange functional with Perdew−Wang 1991 correlation functional; UPW91PW91 = unrestricted Perdew−Wang 1991 exchange functional with Perdew−Wang 1991 correlation functional. [b] Gas phase, ref 7. [c] Ne matrix, ref 2.

CI methods, Knight et al.[11] obtained 776 and 42 MHz for A_{iso}(Al) and A_{dip}(Al), respectively. Engels et al.,[16] with PWP86/IGLO-III, found 696.6 and 52.0 MHz for these quantities.

Both methods and basis sets used in the calculation of HFCCs need some closer examination. In the review article by Engels et al.,[16] it is shown that DFT methods with gradient corrections perform in general better for the calculation of HFCCs than local density approximations. However, in the specific case of this study, it was found preferable to use a method that replicates the experimental gas-phase HFCC of AlO, which then serves as a reference for the changes introduced by the addition of Rg atoms. As far as the basis set is concerned, large Pople-type basis sets have been compared with correlation-consistent basis sets in a study on the HFCCs of the thioformyl radical[27] and found to give equally good or better results for the A_{iso}'s. Calculated anisotropic HFCCs are generally less dependent on the choice of DFT method and basis set.[16]

HFCCs listed in the forthcoming tables were obtained with the SVWN functional for AlO and GaO complexes and with B3LYP for BO complexes. For BO, B3LYP results (1057.3 MHz for A_{iso}(B)) are closer to experimental values (A_{iso}(B) = 1027.4 MHz[9]) than SVWN results (A_{iso}(B) = 970.4 MHz), although the differences between various methods are small. For A_{iso}(B) and A_{dip}(B) of BO, Knight et al.[11] obtained 968 and 26 MHz, whereas Engels et al.[16] found 996.5 and 28.5 MHz. The situation for GaO is similar to that of AlO. The SVWN method gives 1466.3 MHz for A_{iso}(Ga), which is close to 1483 MHz observed in Ne matrix. All other theoretical methods investigated lead to inferior A_{iso}(Ga)'s. For example, the results (in MHz) are 641.9 for B3LYP, 1046.9 for UHF, −96.5 for MP2, and −101.3 for CISD.

The models used for the placement of Rg atoms in relation to AlO have been described in paper I. The notation $Rg_n(a,b)$−AlO indicates that there is a total of n Rg atoms, a in axial positions and b in off-axial positions with $a + b = n$. There can be 0 or 2 Rg atoms in axial position. In the case of two axial Rg atoms, one is on the Al and the other on the O side of AlO at a distance R from Al or O. Off-axial Rg atoms always come in multiples of four. For $b = 4$, there is one ring of Rg

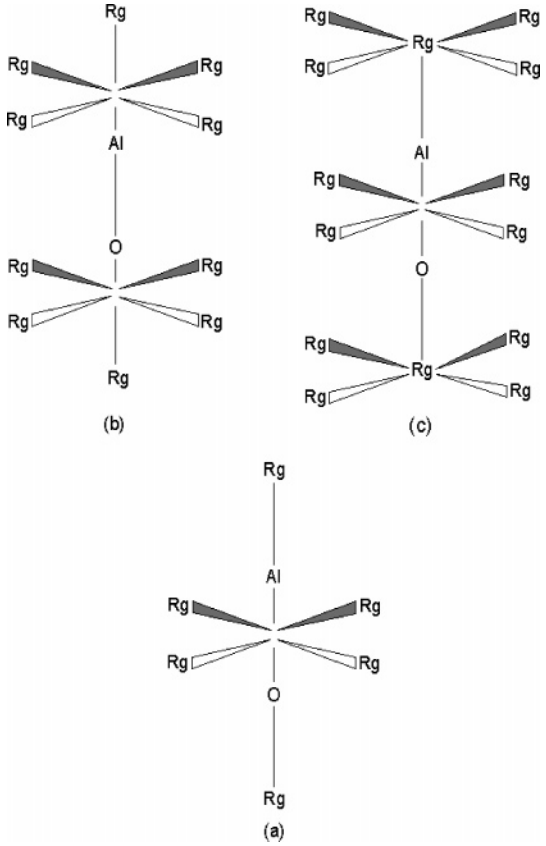

Figure 1. Structures of $Rg_6(2,4)-AlO$ (a), $Rg_{10}(2,8)-AlO$ (b), and $Rg_{14}(2,12)-AlO$ (c).

atoms, with the center of the ring on the AlO axis between Al and O, at a distance of 1.2451 bohr from Al, which corresponds to the center of electronic charge for AlO. (To achieve minimal gauge effects, the electronic charge centroid has been used in the **g**-tensor calculations as coordinate origin.[1] For HFCC calculations, such choice is unimportant but will be used for the sake of consistency with the **g**-tensor models.) With two rings, $b = 8$, the centers of the rings are spaced equally outside of Al and O, such that the distance between the centers is R and at the same time the distance of the Rg atoms from the their respective center on the axis is also R. Finally, for three rings, $b = 12$, the middle ring is placed as for $b = 4$, while the outer rings have their center on the axis at a distance R outside of Al and O, and the distance of the Rg atoms from the center is R. The middle ring is rotated by 45° with the respect to the two outer rings. For BO and GaO complexes, the same models will be used. In the case of BO, the middle ring will be centered at a distance of 1.4736 bohr from the B atom, and for GaO the center is chosen to be 0.7150 bohr from Ga. Both distances correspond to the center of electronic charge for the respective XO molecule.

Diagrams of $Rg_6(2,4)-AlO$, $Rg_{10}(2,8)-AlO$, and $Rg_{14}(2,12)-AlO$ complexes are shown in Figure 1. To make the computations tractable, the models were kept one-dimensional with respect to the distance. The same distance is used for spacings of axial Rg atoms from X and O and for off-axial Rg atoms from the axis.

Results

In Table 3, calculated HFCCs are given for the Ne−AlO systems as a function of the distance R with $R = 4$, 5, 6, 9, and 12 bohr. The corresponding information for Ar−AlO systems is shown in Table 4.

TABLE 3: Hyperfine Coupling Constants (MHz) for Ne−AlO Complexes with Distance R in bohr[a]

complex	R	A_{iso}(Al)	A_{dip}(Al)	A_{iso}(O)	A_{dip}(O)
$Ne_2(2,0)-AlO$	4	828.8	49.0	14.4	−57.2
	5	820.4	56.1	17.3	−54.8
	6	773.6	57.2	18.6	−54.1
	9	752.0	57.5	19.2	−54.1
	12	751.8	57.5	19.2	−54.1
$Ne_4(0,4)-AlO$	4	667.2	61.5	11.1	−46.9
	5	742.1	58.4	17.6	−52.1
	6	757.3	57.4	19.0	−53.5
	9	755.9	57.4	19.2	−54.0
	12	754.5	57.4	19.2	−54.1
$Ne_6(2,4)-AlO$	4	852.0	53.7	9.1	−46.9
	5	848.7	57.0	15.7	−51.9
	6	777.1	57.2	18.1	−53.8
	9	755.1	57.3	19.2	−54.0
	12	755.3	57.4	19.2	−54.1
$Ne_8(0,8)-AlO$	4	1012.6	58.7	14.4	−29.9
	5	855.2	58.2	18.2	−48.6
	6	767.3	57.4	18.7	−53.0
	9	743.6	57.6	18.9	−54.1
	12	744.0	57.7	18.9	−54.2
$Ne_{10}(2,8)-AlO$	4	1264.4	52.1	10.3	−33.3
	5	948.5	57.3	16.3	−49.3
	6	789.3	57.1	18.2	−52.9
	9	742.7	57.5	18.9	−54.1
	12	744.1	57.6	18.9	−54.2
$Ne_{12}(0,12)-AlO$	4	818.4	61.8	11.6	−44.7
	5	768.7	57.8	16.7	−51.1
	6	756.4	57.2	18.4	−53.6
	9	752.3	57.5	19.2	−54.2
	12	752.4	57.5	19.2	−54.2
$Ne_{14}(2,12)-AlO$	4	1019.1	54.7	10.0	−45.6
	5	839.4	56.9	15.9	−51.9
	6	786.1	56.9	17.9	−53.3
	9	748.7	57.5	18.7	−54.5
	12	750.2	57.5	19.2	−54.3
AlO		742.4	57.7	19.2	−54.4

[a] SVWN/6-311+G(3d,f) results.

It is seen that A_{iso}(Al) for both Ne−AlO and Ar−AlO complexes is always larger than that of free AlO (742.4 MHz, given at bottom of Tables 3 and 4). It generally decreases with increasing distance, with the exception of the Ne_4-AlO series, where it increases. The values at 9 and 12 bohr are close to those of free AlO. In very few instances, the largest value is obtained at 5 bohr. Deviation of A_{iso}(Al) from that of pure AlO is larger for Ar (Table 4) than for Ne (Table 3) complexes at every distance.

Isotropic hyperfine coupling constants of ^{17}O are usually smallest at 4 bohr, rising to 19.2 MHz at 12 bohr, the value for free AlO. As will be shown later, the s-spin density on O in AlO and Rg−AlO is extremely small, about 0.4%, while the s-spin density of Al in AlO is about 19%.

Overall, changes in the dipolar HFCCs are usually smaller than those in the isotropic values. For Ne−AlO complexes, A_{dip}(Al) and A_{dip}(O) stay fairly constant, with possible exceptions at the short distances. For Ar−AlO systems, larger deviations are observed at 4 and sometimes 5 bohr for both A_{dip}(Al) and A_{dip}(O).

For the largest Ne cluster, $Ne_{14}-AlO$, A_{iso}(Al) changes from 1019.1 MHz at 4 bohr to 750.2 MHz at 12 bohr, A_{dip}(Al) from 54.7 to 57.5 MHz, A_{iso}(O) from 10.0 to 19.2 MHz, and A_{dip}(O) from −45.6 to −54.3 MHz. For the $Ar_{14}-AlO$ complex, the corresponding ranges are (in MHz) 1653.8 to 752.2 for A_{iso}(Al), 34.3 to 57.5 for A_{dip}(Al), 0.9 to 19.1 for A_{iso}(O), and −9.2 to −54.1 for A_{dip}(O). In all cases, the 12 bohr numbers are close to those of free AlO. At 4 bohr, the Ar values for

TABLE 4: Hyperfine Coupling Constants (MHz) for Ar−AlO Complexes with Distance *R* in bohr[a]

complex	*R*	A_{iso}(Al)	A_{dip}(Al)	A_{iso}(O)	A_{dip}(O)
Ar_2(2,0)−AlO	4	662.5	30.8	10.0	−55.7
	5	897.4	49.4	13.2	−52.9
	6	825.9	55.4	16.9	−53.2
	9	747.5	57.4	19.0	−54.1
	12	746.3	57.6	19.1	−54.3
Ar_4(0,4)−AlO	4	1224.5	54.1	1.2	−10.2
	5	831.0	58.6	11.0	−40.3
	6	786.3	57.4	17.3	−50.1
	9	753.1	57.4	19.2	−54.1
	12	748.1	57.6	19.1	−54.3
Ar_6(2,4)−AlO	4	1359.4	30.7	0.23	−10.4
	5	1047.6	52.8	9.0	−40.1
	6	861.1	55.7	15.4	−49.6
	9	752.4	57.2	19.1	−53.9
	12	750.3	57.5	19.1	−54.2
Ar_8(0,8)−AlO	4	1430.3	40.0	−10.5	−0.93
	5	1214.0	54.2	11.1	−29.2
	6	881.1	56.3	17.0	−47.2
	9	745.6	57.4	18.8	−53.9
	12	744.6	57.7	18.9	−54.1
Ar_{10}(2,8)−AlO	4	1273.9	19.7	−13.9	−5.7
	5	1474.6	50.9	5.3	−32.9
	6	962.3	54.9	14.7	−47.1
	9	745.1	57.3	18.7	−53.7
	12	744.7	57.6	18.9	−54.1
Ar_{12}(0,12)−AlO	4	1619.4	56.1	0.29	−11.1
	5	900.5	57.9	10.7	−39.1
	6	780.3	57.0	16.8	−49.8
	9	754.4	57.4	19.2	−54.0
	12	752.2	57.5	19.1	−54.2
Ar_{14}(2,12)−AlO	4	1653.8	34.3	0.9	−9.2
	5	1112.3	52.4	8.9	−38.8
	6	862.5	55.6	15.2	−49.4
	9	754.7	57.2	19.2	−53.8
	12	752.2	57.5	19.1	−54.1
AlO		742.4	57.7	19.2	−54.4

[a] SVWN/6-311+G(3d,f) results.

TABLE 6: Hyperfine Coupling Constants (MHz) for Ar−BO Complexes with Distance *R* in bohr[a]

complex	*R*	A_{iso}(B)	A_{dip}(B)	A_{iso}(O)	A_{dip}(O)
Ar_2(2,0)−BO	4	1032.9	22.3	−24.4	−23.2
	5	1086.2	26.5	−17.3	−21.7
	6	1071.6	27.3	−13.2	−21.4
	9	1057.9	27.4	−11.4	−21.3
	12	1057.4	27.4	−11.3	−21.3
Ar_4(0,4)−BO	4	1187.3	24.6	12.0	−13.0
	5	1080.3	27.3	1.1	−19.5
	6	1063.6	27.5	−8.4	−21.0
	9	1057.5	27.4	−11.4	−21.3
	12	1057.3	27.4	−11.3	−21.3
Ar_6(2,4)−BO	4	1247.8	22.9	7.5	−16.4
	5	1123.5	26.8	−3.7	−20.1
	6	1079.3	27.4	−10.2	−21.0
	9	1058.3	27.4	−11.4	−21.3
	12	1057.5	27.4	−11.4	−21.3
Ar_8(0,8)−BO	4	1309.8	25.0	−14.9	−7.2
	5	1140.1	27.5	−10.6	−17.4
	6	1079.0	27.5	−11.9	−20.5
	9	1058.2	27.4	−11.4	−21.3
	12	1057.5	27.4	−11.3	−21.3
Ar_{10}(2,8)−BO	4	1381.7	23.9	−23.3	−10.6
	5	1185.9	27.4	−15.3	−18.4
	6	1094.2	27.5	−13.6	−20.6
	9	1058.9	27.4	−11.5	−21.3
	12	1057.6	27.4	−11.4	−21.3
Ar_{12}(0,12)−BO	4	1245.5	26.4	11.1	−13.8
	5	1092.8	27.4	0.3	−19.4
	6	1066.1	27.5	−8.7	−20.9
	9	1057.8	27.4	−11.4	−21.3
	12	1057.4	27.4	−11.3	−21.3
Ar_{14}(2,12)−BO	4	1242.9	22.6	6.1	−13.4
	5	1134.8	26.8	−4.4	−19.5
	6	1083.1	27.4	−10.6	−20.9
	9	1058.6	27.4	−11.5	−21.3
	12	1057.5	27.4	−11.4	−21.3
BO		1057.3	27.4	−11.3	−21.3

[a] B3LYP/6-311+G(3d,f) results.

A_{iso}(Al) and A_{dip}(Al) are 1.5−2 times those for Ne, while the A_{iso} and A_{dip} values for O are even higher multiples of the Ne values.

In Tables 5 and 6, isotropic and dipolar HFCCs are shown for the Ne−BO and Ar−BO systems, respectively. A cursory survey of the results shows that deviations from the free BO values, given at the bottom of these tables, are much smaller than those for the corresponding Rg−AlO systems discussed earlier. As the distance *R* increases, A_{iso}(B) is positive and decreasing, while A_{iso}(O), being negative, becomes more negative. A_{dip}(B) and A_{dip}(O) show only small changes with increasing distance, not always in a consistent manner.

For the Ne_{14}−BO system, with increasing distance, A_{iso}(B) moves from 1198.7 to 1057.3 MHz, A_{dip}(B) from 27.2 to 27.4 MHz with a maximum of 27.5 at 5 bohr, A_{iso}(O) from −5.9 to −11.3 MHz, and A_{dip}(O) stays within 0.1 MHz of the free BO value of −21.3 MHz. For Ar_{14}−BO complexes, the values for the 4−12 bohr range, in MHz, are 1242.9 to 1057.5 for A_{iso}(B), 22.6 to 27.4 for A_{dip}(B), 6.1 to −11.4 for A_{iso}(O), and −13.4 to −21.3 for A_{dip}(O).

One notices that A_{iso}(O) is negative for BO and Rg−BO complexes (except at 4 and 5 bohr for some systems), while it is positive for AlO and the Rg−AlO systems. This point will be discussed later.

So far, only the general trends for A_{iso} and A_{dip} as a function of the distance have been considered. It is of interest to study the changes as the system size increases from two Rg atoms in Rg_2−AlO or Rg_2−BO to 14 Rg atoms in Rg_{14}−AlO and Rg_{14}−BO. In addition, in the previous paper on the changes of **g**-tensors for Rg−AlO systems, different trends were observed for the addition of axial and off-axial Rg atoms. As will be seen, such trends also emerge for the HFCCs. Since it would be difficult to compare the series at all five distances, values at 5 bohr only have been selected for further analysis. The choice of 5 bohr, while somewhat arbitrary, reflects the conclusions drawn in paper I that the largest deviations of $\mathbf{g}_\perp$ from that of AlO occur at distances of 5−6 bohr. While for HFCCs the largest deviations from free AlO and BO values are observed mostly at 4 bohr, the interactions of Rg atoms with AlO and BO at such a short distance are very strong, corresponding to forced high-energy systems that could not easily be achieved in nature. A_{iso}(Al), A_{iso}(B), and A_{iso}(O) numbers at 5 bohr are shown in Table 7 for Ne−AlO, Ar−AlO, Ne−BO, and Ar−BO complexes. This table also contains the percentage deviations of A_{iso} (in parentheses) from the values applicable to free AlO or BO.

In discussion of Table 7, it may be useful to look at isotropic HFCCs of Al and B first. The following observations can be made: (i) For both Rg−AlO and Rg−BO systems, A_{iso}(Al,B) is always larger for Ar than for Ne, corresponding to a larger percent deviation from the AlO/BO values. For example, for Rg_{10}−AlO, A_{iso}(Al) (in MHz) is 948.5 for Ne (27.8%) and 1474.6 for Ar (98.6%). For Rg_{10}−BO, A_{iso}(B) is 1112.6 for Ne (5.2%) and 1185.9 for Ar (12.2%). (ii) For the Rg−AlO and

TABLE 5: Hyperfine Coupling Constants (MHz) for Ne−BO Complexes with Distance *R* in bohr[a]

complex	*R*	A_{iso}(B)	A_{dip}(B)	A_{iso}(O)	A_{dip}(O)
Ne_2(2,0)−BO	4	1114.6	26.8	−18.3	−23.1
	5	1080.5	27.5	−13.2	−21.7
	6	1062.4	27.4	−11.8	−21.4
	9	1057.5	27.4	−11.3	−21.3
	12	1057.3	27.4	−11.3	−21.3
Ne_4(0,4)−BO	4	1078.5	26.9	0.1	−20.3
	5	1060.5	27.5	−8.6	−21.2
	6	1058.4	27.4	−11.0	−21.3
	9	1057.2	27.4	−11.3	−21.3
	12	1057.3	27.4	−11.3	−21.3
Ne_6(2,4)−BO	4	1155.7	26.5	−4.7	−22.0
	5	1085.2	27.6	−10.4	−21.5
	6	1063.6	27.5	−11.4	−21.3
	9	1057.4	27.4	−11.3	−21.3
	12	1057.3	27.4	−11.3	−21.3
Ne_8(0,8)−BO	4	1182.2	28.5	−7.4	−16.8
	5	1087.1	27.8	−11.4	−20.6
	6	1063.1	27.5	−11.6	−21.2
	9	1057.4	27.4	−11.3	−21.3
	12	1057.3	27.4	−11.3	−21.3
Ne_{10}(2,8)−BO	4	1290.0	29.1	−13.3	−18.8
	5	1112.6	28.0	−13.2	−21.0
	6	1068.2	27.5	−12.0	−21.3
	9	1057.6	27.4	−11.4	−21.3
	12	1057.3	27.4	−11.3	−21.3
Ne_{12}(0,12)−BO	4	1109.5	27.3	−1.1	−20.3
	5	1063.4	27.5	−8.9	−21.1
	6	1059.2	27.4	−11.0	−21.3
	9	1057.3	27.4	−11.3	−21.3
	12	1057.3	27.4	−11.3	−21.3
Ne_{14}(2,12)−BO	4	1198.7	27.2	−5.9	−21.3
	5	1091.8	27.2	−10.8	−21.4
	6	1064.9	27.5	−11.5	−21.3
	9	1057.5	27.4	−11.4	−21.3
	12	1057.3	27.4	−11.3	−21.3
BO		1057.3	27.4	−11.3	−21.3

[a] B3LYP/6-311+G(3d,f) results.

Rg−BO series, A_{iso}(Al,B) is always larger (both in magnitude and in percent deviation from the AlO/BO values) for series that have axial Rg atoms, like Rg_6, Rg_{10}, and Rg_{14}, than for the corresponding series having off-axial Rg atoms only, like Rg_4, Rg_8, and Rg_{12}. Examples are 948.5 MHz for Ne_{10}−AlO vs 855.2 MHz for Ne_8−AlO and 1112.6 MHz for Ne_{10}−BO vs 1087.1 MHz for Ne_8−BO.

Observations from Table 7 for A_{iso}(O) are as follows: (i) For Rg−AlO systems, A_{iso}(O) is always larger in magnitude for Ne than for Ar. Since the A_{iso}(O) values for Rg−AlO systems are *smaller* than those for AlO, this corresponds to a smaller deviation from the AlO values for Ne than for Ar, as one would expect. For Rg_{10}−AlO, A_{iso}(O) is 16.3 MHz for Ne and 5.3 MHz for Ar, corresponding to −15.1% vs −72.4% deviations from the AlO value. (ii) For Rg−BO complexes, A_{iso}(O) for Ne may be larger or smaller in magnitude than that of Ar; however, in all cases, the percentage deviation of A_{iso}(O) from that of free BO is larger for Ar than for Ne. In the case of Rg_{10}−BO, A_{iso}(O) for Ne is −13.2 MHz and that for Ar is −15.3 MHz, corresponding to deviations of 16.8% vs 35.4%. (iii) A_{iso}(O) for AlO and all Rg−AlO systems is positive, while it is negative for BO and all Rg−BO systems. The last point implies that for AlO and Rg−AlO, the s-spin density on O is negative, but it is positive for BO and its complexes, since the magnetic moment of ^{17}O is negative.

Using a distance of 6 rather than 5 bohr would lead to very similar conclusions, except that the deviations from the AlO/BO values are in general not as large as at 5 bohr.

Values for the dipolar HFCCs at 5 bohr have been collected in Table 8. Again, percent deviations from the A_{dip} values of AlO and BO are given. In the discussion below, A_{dip}(Al,B) will be dealt with first, followed by A_{dip}(O).

For A_{dip}(Al,B), one can state the following points: (i) For the Ne−AlO systems, the A_{dip}(Al) values lie between 56.1 and 58.4 MHz, all within 2.4% of the AlO value. The Ar−AlO values of A_{dip}(Al) lie between 49.4 and 57.9 MHz, within 14.1% of the AlO value. In each case, except for Rg_4, the deviations from the free AlO value are larger for Ar than for Ne complexes. For Rg−BO complexes, A_{dip}(B) lies between 27.2 and 28.0 MHz, within 2.2% of the BO value of 27.4 MHz. The deviations from this number are, in general, not larger for Ar than for Ne. All Ar values are (slightly) lower than corresponding Ne values. (ii) For the Ar−AlO systems, larger deviations of A_{dip}(Al) from the AlO values can be noticed for systems with axial Ar atoms, such as Rg_6, Rg_{10}, and Rg_{14}. For Ne−AlO and Rg−BO systems, no systematic differences can be seen between complexes having axial plus off-axial or off-axial Rg atoms only.

The Ne−AlO values for A_{dip}(O) lie between −48.6 and −54.8 MHz, mostly below (in magnitude) the AlO value of −54.4 MHz. The maximum deviation is 10.7%. For Ar−AlO complexes, A_{dip}(O) lies between −29.2 and −52.9 MHz with a maximal deviation of 46.3%. The deviations from the AlO value are in all cases larger for Ar than for Ne systems.

For the Rg−BO systems, A_{dip}(O) for Ne ranges from −20.6 to −21.7 MHz, within 3.3% of the BO value, and for Ar from −17.4 to −21.7 MHz, within 18.5% of the BO value. The Ar values are always lower than the Ne values (except for Rg_2), having larger percent deviations from BO values.

For GaO and its Rg complexes, HFCCs have been obtained only for Rg_{12} and Rg_{14} systems. They are displayed in Table 9 and will in the following section be used for comparison with the AlO and BO results.

Discussion

It has been shown that changes in HFCCs are much larger for Ar−XO than for Ne−XO systems. When Rg−AlO at 5 bohr (Table 7) is used as an example, A_{iso}(Al) is up to 1.5 times larger for Ar than Ne complexes, and A_{iso}(O) may differ by a factor up to 3. Matrix effects for AlO and GaO are much larger than those for BO, which, while still discernible, are quite small, the largest deviations of A_{iso}(B) from that of free BO being 12.2% (at 5 bohr).

In Table 10, experimental HFCCs for AlO in the gas phase, as well as in Ne, Ar, and Kr matrixes, as far as available, are contrasted with our theoretical results for AlO and for the largest Rg−AlO systems, Rg_{12}−AlO and Rg_{14}−AlO. Calculated Kr_{12}−AlO and Kr_{14}−AlO results have been included in this table. As discussed earlier, the experimental gas-phase A_{iso}(Al) and A_{dip}(Al) values of AlO lie very close to the calculated ones when the SVWN functional is used. The experimental A_{iso}(Al) increases from the gas phase (738.0 MHz) to Ne (766 MHz), Ar (899 MHz), and Kr (920 MHz). For the Ne matrix, the experimental A_{iso}(Al) corresponds to our Ne_{12} value at 5 bohr and to the Ne_{14} results between 6 and 9 bohr. For the Ar matrix, the experimental value matches the theoretical Ar_{12} result for *R* again at 5 bohr, and the Ar_{14} result for *R* lying between 5 and 6 bohr. The situation for Kr_{12} and Kr_{14} is very similar. The experimental A_{iso}(Al) for AlO in a Kr matrix matches the theoretical Kr_{12} value for *R* between 5 and 6 bohr and the Kr_{14}

TABLE 7: Isotropic Hyperfine Coupling Constants (MHz) at $R = 5$ bohr for Rg−AlO and Rg−BO Complexes with Percent Deviations from the Corresponding AlO and BO Values in Parentheses[a]

	AlO				BO			
	Ne		Ar		Ne		Ar	
	A_{iso}(Al)	A_{iso}(O)	A_{iso}(Al)	A_{iso}(O)	A_{iso}(B)	A_{iso}(O)	A_{iso}(B)	A_{iso}(O)
Rg_2(2,0)	820.4 (10.5)	17.3 (−9.9)	897.4 (20.9)	13.2 (−31.3)	1080.5 (2.2)	−13.2 (16.8)	1086.2 (2.7)	−17.3 (53.3)
Rg_4(0,4)	742.1 (0.0)	17.6 (−8.3)	786.3 (5.9)	17.3 (−9.9)	1060.5 (0.3)	−8.6 (−23.9)	1080.3 (2.2)	1.1 (−90.3)
Rg_6(2,4)	848.7 (14.3)	15.7 (−18.2)	1047.6 (41.1)	9.0 (−53.1)	1085.2 (2.6)	−10.4 (−8.0)	1123.5 (6.3)	−3.7 (−67.3)
Rg_8(0,8)	855.2 (15.2)	18.2 (−5.2)	1214.0 (63.5)	11.1 (−42.2)	1087.1 (2.8)	−11.4 (0.9)	1140.1 (7.8)	−10.6 (−6.2)
Rg_{10}(2,8)	948.5 (27.8)	16.3 (−15.1)	1474.6 (98.6)	5.3 (−72.4)	1112.6 (5.2)	−13.2 (16.8)	1185.9 (12.2)	−15.3 (35.4)
Rg_{12}(0,12)	768.7 (3.5)	16.7 (−13.0)	900.5 (21.3)	10.7 (−44.3)	1063.4 (0.6)	−8.9 (−21.2)	1092.8 (3.4)	0.31 (−97.3)
Rg_{14}(2,12)	839.4 (13.1)	15.9 (−17.2)	1112.3 (49.8)	8.9 (−53.6)	1091.8 (3.3)	−10.8 (−4.4)	1134.8 (7.3)	−4.4 (−61.1)
AlO/BO	742.4	19.2	742.4	19.2	1057.3	−11.3	1057.3	−11.3

[a] SVWN/6-311+G(3d,f) results for Rg−AlO; B3LYP/6-311+G(3d,f) results for Rg−BO.

TABLE 8: Dipolar Hyperfine Coupling Constants (MHz) at $R = 5$ bohr for Rg−AlO Complexes (SVWN/6-311+G(3d,f) Results) and Rg−BO Complexes (B3LYP/6-311+G(3d,f) Results) with Percent Deviations from the AlO and BO Values in Parentheses

	AlO				BO			
	Ne		Ar		Ne		Ar	
	A_{dip}(Al)	A_{dip}(O)	A_{dip}(Al)	A_{dip}(O)	A_{dip}(B)	A_{dip}(O)	A_{dip}(B)	A_{dip}(O)
Rg_2(2,0)	56.1 (−2.4)	−54.8 (0.7)	49.4 (−14.1)	−52.9 (−2.8)	27.5 (0.4)	−21.7 (1.6)	26.5 (−3.3)	−21.7 (1.6)
Rg_4(0,4)	58.4 (1.6)	−52.1 (−4.2)	57.4 (−0.2)	−50.1 (−7.9)	27.5 (0.4)	−21.2 (0.0)	27.3 (−0.4)	−19.5 (−8.7)
Rg_6(2,4)	57.0 (−0.9)	−51.9 (−4.6)	52.8 (−8.2)	−40.1 (−26.3)	27.6 (0.7)	−21.5 (0.9)	26.8 (−2.2)	−20.1 (−5.9)
Rg_8(0,8)	58.2 (1.2)	−48.6 (−10.7)	54.2 (−5.7)	−29.2 (−46.3)	27.8 (1.5)	−20.6 (−3.3)	27.5 (3.7)	−17.4 (−18.5)
Rg_{10}(2,8)	57.3 (−0.3)	−49.3 (−9.4)	50.9 (−11.5)	−32.9 (−39.5)	28.0 (2.2)	−21.0 (−1.6)	27.4 (0.2)	−18.4 (−13.8)
Rg_{12}(0,12)	57.8 (0.5)	−51.1 (−6.1)	57.9 (0.7)	−39.1 (−28.1)	27.5 (0.4)	−21.1 (−0.9)	27.4 (0.0)	−19.4 (−8.9)
Rg_{14}(2,12)	56.9 (−1.0)	−51.9 (−4.6)	52.4 (−8.9)	−38.8 (−28.7)	27.2 (−0.7)	−21.4 (2.3)	26.8 (−2.0)	−19.5 (−8.7)
AlO/BO	57.5	−54.4	57.5	−54.4	27.4	−21.3	27.4	−21.3

TABLE 9: Hyperfine Coupling Constants (MHz) for Ne−GaO and Ar−GaO Complexes with Distance R in bohr[a]

complex	R	A_{iso}(Ga)	A_{dip}(Ga)	A_{iso}(O)	A_{dip}(O)
Ne_{12}(0,12)−GaO	4	1860.1	136.2	13.8	−58.5
	5	1504.1	128.2	19.5	−70.0
	6	1459.9	127.1	20.7	−72.6
	9	1510.6	126.6	21.2	−73.0
	12	1509.9	126.6	21.1	−73.1
Ne_{14}(2,12)−GaO	4	2380.2	127.5	12.9	−61.1
	5	1693.7	127.1	18.8	−70.5
	6	1503.3	126.7	20.5	−72.6
	9	1455.4	127.4	20.7	−73.3
	12	1458.0	127.5	20.6	−73.4
Ar_{12}(0,12)−GaO	4	3664.6	134.0	−0.55	−19.4
	5	1910.1	128.8	13.8	−56.3
	6	1510.2	127.0	19.3	−69.3
	9	1407.1	127.8	20.6	−74.0
	12	1399.3	128.2	20.5	−74.1
Ar_{14}(2,12)−GaO	4	4041.5	88.5	1.6	−17.7
	5	2426.3	119.2	12.4	−56.0
	6	1748.5	123.8	18.5	−68.0
	9	1386.6	127.8	20.4	−74.0
	12	1388.8	128.3	20.4	−74.2
GaO		1466.3	127.4	20.8	−73.2

[a] SVWN/6-311+G(3d,f) results.

TABLE 10: Comparison of Experimental and Theoretical Values for A_{iso} and A_{dip} (MHz) of AlO in Gas Phase and in Rare-Gas Matrixes with Distances R in bohr

	R	A_{iso}(Al)	A_{dip}(Al)	A_{iso}(O)	A_{dip}(O)
gas expt[7]		738.0	56.4		
gas theor		742.4	57.5	19.2	−54.4
Ne expt[2]		766(2)	53.0(7)	2	−50
Ne_{12} theor	4	818.4	61.8	11.6	−44.7
	5	768.7	57.8	16.7	−51.1
	6	756.4	57.2	18.4	−53.6
Ne_{14} theor	5	839.4	56.9	15.9	−51.9
	6	786.1	56.9	17.9	−53.3
	9	748.7	57.5	18.7	−54.5
Ar expt[2]		899(3)	54(1)		
Ar_{12} theor	4	1619.4	56.1	0.29	−11.1
	5	900.5	57.9	10.7	−39.1
	6	780.3	57.0	16.8	−49.8
Ar_{14} theor	5	1112.3	52.4	8.9	−38.8
	6	862.5	55.6	15.2	−49.4
	9	754.7	57.2	19.2	−53.8
Kr expt[2]		920(3)	51(1)		
Kr_{12} theor	4	1803.3	46.5	−3.3	−3.8
	5	1028.1	56.0	7.1	−30.4
	6	829.8	56.1	15.3	−45.5
Kr_{14} theor	5	1250.5	47.2	5.7	−29.2
	6	938.5	53.4	12.9	−44.6
	9	767.7	56.8	19.0	−53.3

result for R slightly beyond 6 bohr. (It has been mentioned earlier that maximal deviations of the **g**-tensor component $\mathbf{g}_\perp$ from that of AlO occur at distances of 5 bohr for Ne and about 6 bohr for Ar when the largest models are used.)

Experimental A_{dip}(Al)'s do not show any systematic trend when they move from Ne to Kr matrixes. They increase from Ne to Ar but decrease from Ar to Kr. Because all three values are similar, it implies that matrix effects do not influence A_{dip}(Al) to any significant extent. The theoretical number for Ne_{12} and Ne_{14} at 5 bohr is 4−5 MHz higher than the experimental value. For the Ar matrix the experimental number lies about 4 MHz below the Ar_{12} value at 5 bohr and corresponds to the Ar_{14} value between 5 and 6 bohr. At a given distance, such as 5 bohr, A_{dip}(Al) for Ar_{14}−AlO is lower than A_{dip}(Al) for Ne_{14}−AlO. For Kr, the experimental value of 51 MHz can be associated with the Kr_{12} numbers for R slightly below 5 bohr and the Kr_{14} numbers for R between 5 and 6 bohr. Experimental numbers for A_{iso} and A_{dip} of O are available only for AlO in Ne matrix. A_{iso}(O) of 2 MHz lies much below any of the calculated values, whereas the experimental A_{dip}(O) of −50 MHz is 1 MHz

below the 5 bohr value of the Ne_{12} complex. From the Ar_{12} data of Table 10, an Ar matrix value for A_{dip}(O) of about −38 MHz is predicted.

For BO, experimental HFCCs measured in the gas phase differ little from those in Ne matrix. This is in agreement with our calculated values, where A_{iso}(B) for Ne_{12} at 5 bohr lies only 6 MHz higher than that of free BO and A_{dip}(B) is virtually unchanged. The observed HFCCs for ^{17}O, however, do not agree with the calculated ones. Both in the gas phase and in Ne matrix, we obtain −9 to −11 MHz for A_{iso}(O) and −21 MHz for A_{dip}(O), compared to observed values of −19 and −12 MHz, respectively. The ZORA results obtained by Belanzoni et al.[15] are similar to ours. Earlier CI results, reported in ref 12, however, find A_{iso}(O) to be −20 MHz, and A_{dip}(O) to be −16 MHz, in much better agreement with the experimental numbers.

Our calculations indicate that HFCCs for BO in an Ar matrix do not differ much from those in an Ne matrix. Using Rg_{12}−BO values at 5 bohr, we predict A_{iso}(B) to be about 30 MHz higher in Ar than in Ne, whereas A_{dip}(B) is about the same.

In Table 1, A_{iso}(Ga) for GaO in Ne matrix is given as 1483 MHz. Since no gas-phase value is available, we can estimate it by comparing the experimental Ne-matrix number with that calculated for Ne_{12}−GaO at 5 bohr, which is 1504 MHz (Table 9). A difference of about 20 MHz applied to the calculated gas-phase value of 1466 MHz predicts an "experimental" gas-phase value of about 1445 MHz. The "experimental" A_{iso}(Ga) in an Ar matrix is then estimated to be about 1890 MHz, arrived at by deducting 20 MHz from the value calculated for Ar_{12}−GaO at 5 bohr, which is 1910 MHz. When again calculated values for Ne_{12}−GaO at 5 bohr are used, A_{dip}(Ga) is 128.2 MHz, in good agreement with the experimental value of 127 MHz. It is seen that A_{dip} values do not change much with distance. For A_{iso}(O) of GaO in Ne matrix, 19.5 MHz is calculated, but 8 MHz is observed. The agreement is better for A_{dip}(O) with −70 MHz predicted versus −77 MHz observed.

Hyperfine coupling constants can be related to the neutral and ionic structures I−III of the XO radicals, I being $X(s^2p^1) + O(s^2p^4)$, II being $X^+(s^2) + O^-(s^2p^5)$, and III being $X^{2+}(s) + O^{2-}(s^2p^6)$. Looking at the atomic open shells, A_{iso}(X) is then due mainly to the doubly ionized structure III, which has an open-shell s orbital on X, and A_{dip}(X) to the neutral structure I with an open p-shell on X. Because there is no open s-shell for the oxygen atom in any of the three structures, a near-zero s-spin density on O is predicted, consistent with our findings. A_{dip}(O) is due mainly to the singly ionized structure II, which has an open p-shell on O.

According to Weltner,[13] free atom A_{iso}'s for assumed 100% s-spin density (s-SD) are (in MHz) 3911 for ^{27}Al, 2547 for ^{11}B, 12210 for ^{69}Ga, and −5263 for ^{17}O. Corresponding A_{dip}'s for 100% p-spin density (p-SD) are 83.1, 63.6, 203.8, and −168.4 MHz. With these data, s and p spin densities have been calculated by the so-called free atom comparison method[8] for the Rg−BO, Rg−AlO, and Rg-GaO complexes. We realize that the reference numbers apply to neutral atoms, whereas charged species are present in the radicals considered here, as outlined on several occasions. However, for qualitative purposes and not knowing the exact amount of contributions from ionic structures, spin density calculations based on hyperfine coupling constants for the neutral atoms should be sufficient.

In Table 11, spin densities calculated by the free atom comparison method are given for the free radicals and for the radicals in their Ne_{14} and Ar_{14} complexes at 5 bohr. It is seen that the s-SD on X of free XO decreases as one goes from B (41.5%) to Al (19.0%) to Ga (12.0%). The s-SD on X is larger in Ne− and Ar−XO complexes than in free XO, indicating that X gains s-spin density. This is in contrast to the p-spin density on X, which is smaller in the complexes than in XO, pointing to a loss of p-spin density on X as XO gets immersed in Ne or Ar atoms. The changes for BO complexes are much smaller than those for AlO or GaO systems. The highest spin densities for Rg−GaO are slightly smaller than those for Rg−AlO complexes.

TABLE 11: Percent Spin Densities (SD) for Rg_{14}−XO (X = B, Al, Ga) at 5 bohr Calculated from Hyperfine Coupling Constants Given in Tables 3−6 and 9 with Percent Deviation (in Parentheses) of A_{Iso} and A_{Dip} from Free XO Values[a]

	s-SD(X) A_{iso}(X)	p-SD(X) A_{dip}(X)	s-SD(O) A_{iso}(O)	p-SD(O) A_{dip}(O)
BO [μ = 2.44 D]	41.5	43.1	0.2	12.6
Ne_{14}−BO	42.9	42.8	0.2	12.7
% deviation	(3.3)	(−0.7)	(−4.4)	(0.5)
Ar_{14}−BO	44.6	42.1	0.1	11.6
% deviation	(7.3)	(−2.0)	(−61.1)	(−8.7)
AlO [μ = 4.30 D]	19.0	69.4	−0.4	32.3
Ne_{14}−AlO	21.5	68.5	−0.3	30.8
% deviation	(13.1)	(−1.0)	(−17.2)	(−4.6)
Ar_{14}−AlO	28.4	63.1	−0.2	23.0
% deviation	(49.8)	(−8.9)	(−53.6)	(−28.7)
Kr_{14}−AlO	32.0	56.8	−0.1	17.3
% deviation	(68.4)	(−18.2)	(−70.3)	(−46.3)
GaO [μ = 3.89 D]	12.0	62.5	−0.4	43.5
Ne_{14}−GaO	13.9	62.4	−0.4	41.9
% deviation	(15.5)	(−0.2)	(−9.6)	(−3.7)
Ar_{14}−GaO	19.9	58.5	−0.2	33.3
% deviation	(65.5)	(−6.4)	(−40.4)	(−23.5)

[a] Dipole moments, μ, of XO are given in the table. Calculated static polarizabilities (bohr^3) along the X−O axis are 19.4 for BO, 55.3 for AlO, and 48.7 for GaO.

The s-spin density on oxygen is very small, 0.2% for BO and −0.4% for AlO and GaO. For AlO and GaO, as well as their Rg−XO systems, the sign of A_{iso}(O) is positive, opposite to that of the O atom, indicating that the β-s-spin density exceeds the α-s-spin density. Due to the smallness of the spin density on O, such reversal in sign may be caused by numerical inaccuracies. For BO and Rg−BO complexes, A_{iso}(O) is negative, as it is for the free atom. For all systems, the s-SD on O is extremely small and does not change much in the process of complex formation. On the other hand, the p-SD on O, being 32.3% for free AlO, gets smaller as XO is embedded in rare gas atoms, indicating that oxygen loses p-spin density as complexes are formed.

From such observations, the following picture emerges: When XO radicals are surrounded by rare gas atoms, spin density gets transferred from p-orbitals, located both on X and O, to s-orbitals located on X. In terms of structures I−III introduced above, structure III, having doubly charged ions, gains at the expense of the neutral and singly ionic structures I and II. In this picture, rare gas atoms cause further ionization of XO, from X^+O^- to X^{2+} O^{2-}.

One may relate the strength of the matrix effect on the various XO radicals to their electric properties such as dipole moment and static polarizability. Dipole moments for BO, AlO, and GaO have been calculated by B3LYP/6-311+G(2d,f). This basis set, rather than 6-311+G(3d,f), was chosen in paper I to obtain a dipole moment for AlO that is close to that obtained by the best available ab initio calculations (4.30 vs 4.24 D).[28] Static polarizabilities were obtained with B3LYP/6-311+G(3d,f). Dipole moments and polarizabilities are listed in Table 11. The dipole moment for GaO, 3.89 D, is slightly smaller than that of AlO. BO has a much smaller dipole moment of 2.44 D.

Polarizabilities are largest along the XO axis, as one expects due to the SOMO being σ_p, with values (in bohr^3) of 19.4 for BO, 55.3 for AlO, and 48.7 for GaO. Similar to dipole moments, AlO has the highest polarizability, closely followed by GaO, with the value for BO being less than one-half that of AlO and GaO. According to such results, GaO should experience a matrix effect similar or slightly below that of AlO. Deviations from free XO HFCCs, displayed in Table 11, essentially confirm such trend. With the Ar_{14} complex at 5 bohr used as example, its A_{iso}(X) differs by 7.3%, 49.8%, and 65.5% from the free BO, AlO, and GaO values, respectively. A_{dip}(X) for this complex differs by −2.0%, −8.9%, and −6.4% from the respective free XO values. An exception is noticed for A_{iso}(O), but as mentioned on several occasions, due to the extremly small s-spin density on O, the calculated A_{iso}(O) are not considered to be reliable. The deviations for A_{dip}(O) are −8.7%, −28.7%, and −23.5% for BO, AlO, and GaO, respectively.

Summary and Conclusion

Hyperfine coupling constants have been calculated for the radicals BO, AlO, and GaO (XO) surrounded by up to 14 Ne or Ar atoms. For AlO, Kr atoms were also included. Strong matrix effects on HFCCs were found for AlO and GaO and weaker ones for BO. Argon complexes always showed larger changes in HFCCs than Ne complexes. In the models used for the complexes, rare gas atoms were placed in one to three rings of four Rg atoms each around the XO axis. Up to two axial Rg atoms, located on either side of XO, were included. The distance of the axial Rg atoms from the X and O atoms and of the ring atoms from the axis was varied from 4 to 12 bohr. At the shortest distance, matrix effects are usually the strongest, as one would expect, whereas they have mostly disappeared at a distance of 12 bohr. Most noticeable are matrix effects for the isotropic A_{iso}(Al) and A_{iso}(Ga), which increase in the presence of Rg atoms.

Experimental A_{iso}'s, available for AlO in Ne, Ar, and Kr matrixes, are close to values calculated with the largest models having 12 and 14 Rg atoms at distances of 5−6 bohr. The best fit for A_{iso}(Al) is obtained for the Rg_{12} complex at 5 bohr with 769 MHz for Ne and 900 MHz for Ar, compared with experimental values of 766 and 899 MHz, respectively. The experimental Kr matrix value corresponds to A_{iso}(Al) calculated for the Kr_{12} complex at 5−6 bohr. Both experimental and theoretical A_{dip}(Al)'s change little when AlO is placed in a matrix environment.

Relatively strong matrix effects for $A_{iso}(^{17}O)$ of AlO, as found in our calculations, cannot be verified due to insufficient experimental information available. In addition, $A_{iso}(^{17}O)$ is very small, corresponding to an s-spin density of less than 1%, and calculated changes due to the interaction with rare gas atoms may not be reliable. For A_{dip}(O) an experimental Ne-matrix value of −50 MHz is matched closely by the Ne_{12} model at 5 bohr. For the Ar-matrix, A_{dip}(O) of −38 MHz is predicted.

The observed weak Ne-matrix effect for BO is well reflected in our calculations, with a 6 MHz increase in A_{iso}(B) observed and calculated when BO in gas phase is taken to a Ne matrix. Another 30 MHz increase in A_{iso}(B) is predicted when it goes from Ne to Ar matrixes. However, there is no agreement between observed and calculated A_{iso}(O) and A_{dip}(O) for BO in Ne matrix.

For GaO, experimental HFCCs are known only for Ne matrix with A_{iso}(Ga) = 1483 MHz and A_{dip}(Ga) = 127 MHz. Based on the calculations, a gas-phase value of 1445 MHz and an Ar-matrix value of 1890 MHz is predicted. A_{dip}(Ga) is not found to change appreciably when going from gas phase to an Ar-matrix.

TABLE 12: Summary of Experimental and Calculated Hyperfine Coupling Constants (MHz) for BO, AlO, and GaO in the Gas Phase and in Rare Gas Matrixes

system	method	A_{iso}(X)	A_{dip}(X)	A_{iso}(O)	A_{dip}(O)
BO, gas	expt	1027.4	27.1		
	calcd	1057.3	27.4	−11.3	−21.3
BO−Ne	expt	1033	25	−19	−12
	calcd	1063.4	27.5	−8.9	−21.1
BO−Ar	calcd	1063[a]	27.4	0.3	−19.4
AlO, gas	expt	738.0	56.4		
	calcd	742.4	57.5	19.2	−54.4
AlO−Ne	expt	766	53.0	2	−50
	calcd	768.7	57.8	16.7	−51.1
AlO−Ar	expt	899	54		
	calcd	900.5	57.9	10.7	−38[a]
AlO−Kr	expt	920	51		
	calcd[b]	930	56	11	−37
GaO, gas	calcd	1445[a]	127.4	20.8	−73.2
GaO−Ne	expt	1483	127	8	−77
	calcd	1504.1	128.2	19.5	−70.7
GaO−Ar	calcd	1890[a]	128.8	13.8	−56.3

[a] Values have been modified, see Discussion. [b] Estimated from Kr_{12}−AlO results halfway between 5 and 6 bohr.

In Table 12, calculated hyperfine data for all three radicals in gas phase and in Ne and Ar matrixes are summarized and contrasted to the experimental findings. The calculated numbers correspond mainly to the results for Rg_{12} models at 5 bohr. Several of the calculated values were adjusted based on experimental results, as outlined in the Discussion.

Some ideas about the role of orientation of the radical in the matrix can be gathered by comparing results obtained for complexes with and without axial Rg atoms, having otherwise the same number of ring atoms. In all cases studied, the addition of axial Rg atoms increases the matrix effect on A_{iso}(X). For Rg−AlO at distances of 5 bohr, A_{iso}(Al) increases by about 100 MHz for Ne complexes and 200 MHz for Ar complexes. For the Rg−GaO systems investigated, the increase is about 200 MHz for Ne and 500 MHz for Ar systems. The reason for the increase in A_{iso}(X) as axial Rg atoms are added to off-axial ones can be related to the parallel component of the polarizability of XO being larger than the perpendicular one.

For all three radicals studied here, the presence of rare gas atoms causes the s-spin density on the metal atom to increase at the expense of p-spin density on both the metal and the oxygen atom. The s-spin density on O is and remains near zero. Since the total spin density has to remain constant, an increase in the s-spin density has always to be compensated by a decrease in the p-spin density, and vice versa, and overall increases/decreases in A_{iso} must be accompanied by overall decreases/increases in A_{dip}. To generalize to other radicals, in addition to s ↔ p spin density conversion, matrix effects may also shift s or p (or d) spin density from one atom to another, in which case increases in A_{iso}/A_{dip} on one atom need to be compensated by decreases on other atoms. The easier it is to convert s to p or p to s spin density or to shift spin densities among atoms, the larger the matrix effect will be. Radical molecules with large dipole moments and polarizabilities are more likely to undergo such changes. In addition, spin density can also be moved to the rare gas atoms. Calculations show that at small distances very small amounts of s- and p-SD (less than 2%) get transferred to rare gas atoms.

It is therefore generally true, as pointed out by Weltner,[13] that HFCCs may increase or decrease in a matrix environment.

In the case of XO radicals studied here, A_{iso}(X) increases, while A_{dip}(X) and A_{dip}(O) decrease. However, for other radicals, A_{iso} may not increase. It was observed,[29] and confirmed by calculations,[20] that A_{iso}(Mg) of Mg^+ ions decreases as one goes from a Ne to an Ar matrix. Also, in examples cited by Ammeter and Schlosnagle,[30] the magnitude of A_{iso} for Al or Ga atoms is smaller in Ar than in Ne matrixes.

In paper I, we noticed that in the presence of rare gases, $\Delta\mathbf{g}_\perp$ increases in magnitude, caused by an increase in $\langle L\rangle$ and $\langle SO\rangle$, and a decrease in ΔE, where the matrix elements $\langle L\rangle$ and $\langle SO\rangle$ are taken between the ground state and low-lying excited states, ΔE being the energy difference between these states. Due to strong contributions to $\Delta\mathbf{g}_\perp$ of AlO from at least two excited states with opposite signs, the reasons for matrix effects on $\Delta\mathbf{g}_\perp$ of AlO are more difficult to formulate than those for hyperfine coupling constants.

It is recognized that the models used here for mimicking rare gas effects on XO molecules are fairly rigid with the distances of all Rg atoms being varied in unison. A more flexible model, allowing for the variation of distances individually, as well as the inclusion of a larger number of Rg atoms, is desirable. However, despite such limitations, the results obtained for HFCCs are reasonable and reflect, to the extent that one can compare, the experimental findings. Based on these models, HFCCs for XO molecules in gas phase and in rare gas matrixes not available experimentally can be estimated and eventually put to the test.

Acknowledgment. The author would like to thank Dr. P. J. Bruna for helpful comments. Financial support by NSERC (Canada) is gratefully acknowledged. Thanks to the Advanced Computational Research Laboratory of this University and Chris MacPhee for providing computer time on the Chorus cluster and for help.

References and Notes

(1) Grein, F. *J. Chem. Phys.* **2005**, *122*, 124504.
(2) Knight, L. B.; Weltner, W. *J. Chem. Phys*. **1971**, *55*, 5066.
(3) Bruna, P. J.; Grein, F. *J. Phys. Chem. A* **2001**, *105*, 3328.
(4) Lushington, G. H.; Bündgen, P.; Grein, F. *Int. J. Quantum Chem*. **1995**, *55*, 377.
(5) Lushington, G. H.; Grein, F. *J. Chem. Phys*. **1997**, *106*, 3292.
(6) Brownridge, S.; Grein, F.; Tatchen, J.; Kleinschmidt, M.; Marian, C. M. J. *J. Chem. Phys.* **2003**, *118*, 9552.
(7) Yamada, C.; Cohen, E. A.; Fujitake, M.; Hirota, E. *J. Chem. Phys*. **1990**, *92*, 2146.
(8) Knight, L. B.; Kirk, T. J.; Herlong, J.; Kaup, J. G. *J. Chem. Phys*. **1997**, *107*, 7011.
(9) Tanimoto, M.; Saita, S.; Hirota, E. *J. Chem. Phys*. **1986**, *84*, 1210.
(10) Knight, L. B.; Easley, W. C.; Weltner, W. *J. Chem. Phys*. **1971**, *54*, 1610.
(11) Knight, L. B.; Wise, M. B.; Davidson, E. R.; McMurchie, L. E. *J. Chem. Phys*. **1982**, *76*, 126.
(12) Knight, L. B.; Herlong, J.; Kirk, T. J.; Arrington, C. A. *J. Chem. Phys*. **1992**, *96*, 5604.
(13) Weltner, W. *Magnetic Atoms and Molecules*; Dover: New York, 1983.
(14) Davidson, E. R. *Int. J. Quantum Chem*. **1998**, *69*, 241.
(15) Belanzoni, P.; van Lenthe, E.; Baerends E. J. *J. Chem. Phys*. **2001**, *114*, 4421.
(16) Engels, B.; Eriksson, L. A.; Lunell, S. *Adv. Quantum Chem*. **1996**, *27*, 297.
(17) Yoshimine, M.; McLean, A. D.; Liu, B. *J. Chem. Phys*. **1973**, *58*, 4412.
(18) Knight, L. B.; Ligon, A.; Woodward, R. W.; Feller, D.; Davidson, E. R. *J. Am. Chem. Soc*. **1985**, *107*, 2857.
(19) Kiljunen, T.; Eloranta, J.; Ahokas, J.; Kuntfu, H. *J. Chem. Phys*. **2001**, *114*, 7144.
(20) Eriksson, L. A. *J. Chem. Phys*. **1995**, *103*, 1050.
(21) Eriksson, L. A.; Wang, J.; Boyd, R. J. *Chem. Phys. Lett*. **1995**, *235*, 422.
(22) Frisch, M. J.; Trucks, G. W.; Schlegel, H. B.; Scuseria, G. E.; Robb, M. A.; Cheeseman, J. R.; Montgomery, J. A., Jr.; Vreven, T.; Kudin, K. N.; Burant, J. C.; Millam, J. M.; Iyengar, S. S.; Tomasi, J.; Barone, V.; Mennucci, B.; Cossi, M.; Scalmani, G.; Rega, N.; Petersson, G. A.; Nakatsuji, H.; Hada, M.; Ehara, M.; Toyota, K.; Fukuda, R.; Hasegawa, J.; Ishida, M.; Nakajima, T.; Honda, Y.; Kitao, O.; Nakai, H.; Klene, M.; Li, X.; Knox, J. E.; Hratchian, H. P.; Cross, J. B.; Bakken, V.; Adamo, C.; Jaramillo, J.; Gomperts, R.; Stratmann, R. E.; Yazyev, O.; Austin, A. J.; Cammi, R.; Pomelli, C.; Ochterski, J. W.; Ayala, P. Y.; Morokuma, K.; Voth, G. A.; Salvador, P.; Dannenberg, J. J.; Zakrzewski, V. G.; Dapprich, S.; Daniels, A. D.; Strain, M. C.; Farkas, O.; Malick, D. K.; Rabuck, A. D.; Raghavachari, K.; Foresman, J. B.; Ortiz, J. V.; Cui, Q.; Baboul, A. G.; Clifford, S.; Cioslowski, J.; Stefanov, B. B.; Liu, G.; Liashenko, A.; Piskorz, P.; Komaromi, I.; Martin, R. L.; Fox, D. J.; Keith, T.; Al-Laham, M. A.; Peng, C. Y.; Nanayakkara, A.; Challacombe, M.; Gill, P. M. W.; Johnson, B.; Chen, W.; Wong, M. W.; Gonzalez, C.; Pople, J. A. *Gaussian 03*, revision B.04; Gaussian Inc.: Wallingford, CT, 2004.
(23) Huber, K. P.; Herzberg, G. *Molecular Spectra and Molecular Structure, IV. Constants of Diatomic Molecules*; New York, 1979.
(24) Karna, S. P.; Grein, F. *J. Mol. Spectrosc*. **1987**, *122*, 356−364.
(25) Slater, J. C. *Quantum Theory of Molecules and Solids*; McGraw-Hill: New York, 1967; Vol. 3.
(26) Vosko, S. H.; Wilk, L.; Nusair, M. *Can. J. Phys*. **1980**, *58*, 1200.
(27) Petraco, N. D. K.; Wesolowski, S. S.; Leininger, M. L.; Schaefer, H. F., III *J. Chem. Phys*. **2000**, *112*, 6245.
(28) Zenouda, C.; Blottiau, P.; Chambaud, G.; Rosmus. P. *J. Mol. Struct. (THEOCHEM)* **1999**, *458*, 61.
(29) Knight, L. B.; Cleveland, C. B.; Frey, R. F.; Davidson, E. R. *J. Chem. Phys.* **1994**, *100*, 7867.
(30) Ammeter, J. H.; Schlosnagle, D. C. *J. Chem. Phys*. **1973**, *59*, 4784.